

A Dynamic Fountain Model for Lunar Dust

Timothy J. Stubbs, Richard R. Vondrak, and William M. Farrell

*Laboratory for Extraterrestrial Physics, NASA Goddard Space Flight Center, Greenbelt, MD
20771, USA*

Timothy.J.Stubbs.1@gssc.nasa.gov

Accepted for publication in *Advances in Space Research*, April 2005.

Abstract

There is much evidence to show that lunar “horizon glow” and “streamers” observed at the terminator are caused by sunlight scattered by dust grains originating from the surface. The dust grains and lunar surface are electrostatically charged by the Moon’s interaction with the local plasma environment and the photoemission of electrons due to solar UV and X-rays. This effect causes the like-charged surface and dust particles to repel each other, and creates a near-surface electric field. Previous models have explained micron-sized dust observed at ~10 cm above the surface, by suggesting that charged grains “levitate” in the local electric field; however this cannot account for observations of 0.1 μm -scale grains at ~100 km altitude. In order to explain the high-altitude dust observations, we propose a dynamic “fountain” model in which charged dust grains follow ballistic trajectories, subsequent to being accelerated upward through a narrow sheath region by the surface electric field. These dust grains could affect the optical quality of the lunar environment for astronomical observations and interfere with exploration activities.

Keywords: Lunar regolith; dust grains; lunar horizon glow; lunar surface charging; dust dynamic fountain model.

1. Introduction

During the Apollo era of exploration it was discovered that sunlight was scattered at the terminators giving rise to “horizon glow” and “streamers” above the lunar surface (e.g., McCoy and Criswell, 1974; Rennilson and Criswell, 1974). This was observed from the dark side of the Moon during sunset and sunrise by both surface landers and astronauts in orbit. In fact, some of the most revealing astronaut observations were not captured by camera, but recorded in their log books, an example of which is shown in Fig. 1. These observations were quite unexpected, as the Moon was thought to be a pristine environment with a negligible atmosphere or exosphere. Subsequent investigations have shown that the sunlight was most likely scattered by electrostatically charged dust grains originating from the surface (Criswell, 1973; McCoy, 1974; Rennilson and Criswell, 1974; Berg et al., 1976; Zook and McCoy, 1991). It has since been demonstrated that this dust population could have serious implications for astronomical observations from the lunar surface (Murphy and Vondrak, 1993).

The lunar surface is composed of rocks and regolith, where regolith is a soil-like layer above the bedrock which has been generated by small meteoritic impacts (Heiken et al., 1991). The regolith particles range in size from centimeters to submicron scales; the smaller particles are often referred to as either lunar fines or lunar dust (Heiken et al., 1991). The lunar surface, as described above, is electrostatically charged by the Moon’s large-scale interaction with the local plasma environment and the photoemission of electrons due to solar ultra-violet (UV) light and X-rays (Manka, 1973). The like-charged surface and dust grains then act to repel each other, such that under certain conditions the dust grains are lifted above the surface (Criswell, 1973; McCoy, 1974; Rennilson and Criswell, 1974).

Criswell (1973) argued that horizon glow (HG) observed by the Surveyor-7 lander was caused by electrostatically levitated dust grains with radii $\approx 5 \mu\text{m}$. These grains reached heights of 3 to 30 cm above rocks and surface irregularities in the terminator region, as illustrated in Fig. 2a. He suggested that a large electrostatic field would be generated by high-energy photoelectrons emitted from directly illuminated surfaces, thus forming a stable multipole charge distribution between light and dark areas. The HG light was scattered by large sphere (Fraunhofer) diffraction from dust with line-of-sight column concentrations of $\sim 50 \text{ grains cm}^{-2}$; this was further discussed by Rennilson and Criswell (1974) in relation to observations from

other Surveyor landers. Criswell (1973) and Rennilson and Criswell (1974) both pointed out that the observed HG was almost 10^7 times too bright to be explained by secondary ejecta from micro-meteoroid impacts.

McCoy and Criswell (1974) examined astronaut sketches of spacecraft sunrise, which showed HG and streamers above the lunar surface (e.g., see Fig. 1). These streamers varied on timescales of seconds to minutes indicating that they were produced by light scattering in the lunar vicinity – as opposed to streamers emanating from the Sun (K-corona) which vary on timescales of hours to days – and the scattering particles appeared to be present sporadically. Fig. 3 shows the schematic from McCoy and Criswell (1974) depicting the physical situation which is consistent with the visual observations sketched in Fig. 1. The astronaut observations are important as they could view HG when the Sun was close to the horizon without fear of damaging optics or saturating photographic film, and as such they are the only record of this phenomenon (Zook and McCoy, 1991). McCoy (1976) analyzed excess brightness in 70 mm photographs of the solar corona above the lunar terminator taken from orbit during the Apollo 15 and 17 missions. The excess brightness displayed circular symmetry above the lunar horizon and decayed rapidly in intensity with altitude. He argued that this could not be accounted for by a co-orbiting cloud of spacecraft contaminants. Instead, like McCoy and Criswell (1974), he concluded that it must be due to a variable lunar “atmosphere” of $\sim 0.1 \mu\text{m}$ dust extending to altitudes in excess of 100 km, which was created by some unknown electrostatic suspension mechanism.

The Lunar Ejecta and Meteorites (LEAM) experiment was placed on the Moon during the Apollo 17 mission in order to directly measure the impact of cosmic dust on the lunar surface (Berg et al., 1976). However, the bulk of the events registered by this experiment were not hypervelocity impacts by cosmic dust, but were instead lower velocity impacts attributed to the transport of electrostatically charged lunar dust. The dust impacts were observed to peak around the terminator regions, thus indicating a relationship with the HG observations.

Further examination of the Apollo 17 astronaut sketches by Zook and McCoy (1991) and comparison with their light scattering model showed that the observed HG had a scale height of ~ 10 km (assuming dust density decreases exponentially above the surface). Comparison with this

model again showed that the glow was indigenous to the Moon and not caused by a cloud of contaminants from the spacecraft. They also argued that horizon glow is unlikely to be caused by gases in the lunar exosphere. The two main gases present are sodium and potassium with scale heights of ~ 120 and ~ 90 km, respectively, which are inconsistent with modeling results discussed above. Also, the vapour brightnesses of these gases are likely below the threshold of visibility to the unaided human eye.

Evidence for the occurrence of horizon glow and streamers above the lunar terminator, and their being caused by electrostatically charged lunar dust, is quite compelling. Here we present a dynamic “fountain” model, as illustrated in Fig. 2b, which can explain how submicron dust is able to reach altitudes of up to ~ 100 km above the lunar surface. Previous static dust levitation models are most applicable to the heavier micron-sized grains in close proximity to the surface, but they cannot explain the presence of extremely light grains at high altitudes. If we relax the static constraint applied to previous models, and instead assume that the grains are in constant motion (under the action of dynamic forces), a new picture emerges for the behaviour of submicron lunar dust. In section 2 we describe the dust grain fountain concept and detail the assumptions and equations used in the model. The model results are presented in section 3 and discussed in section 4. Section 5 gives a brief summary and the conclusions.

2. Dynamic dust grain fountain concept and model

Fig. 2 shows a schematic comparing (a) the static levitation concept, as suggested by Criswell (1973) and others, with (b) the evolution of a dust grain in our dynamic fountain model. In the levitation model the dust grain finds a point near the surface where the electrostatic force (F_q) and gravitational force (F_g) acting on it are about equal and opposite, and is thus suspended. In the dynamic fountain model, once the dust grain has attained sufficient charge to overcome lunar gravity and any cohesive forces (F_c), i.e., $F_q > F_g + F_c$, it leaves the lunar surface. It is subsequently accelerated upward through a sheath region with a height of order the plasma Debye length, λ_D . As the dust grain is so small, the gravitational force acting on it is almost negligible in comparison with the initial electrostatic acceleration. The dust grain leaves the sheath region with an upward velocity of V_{exit} and follows a near-parabolic trajectory back toward the lunar surface since the main force acting on it now is gravity.

The first parameter we need to calculate is the electrostatic surface potential, ϕ_s , and we do this using the method and equations given in Manka (1973). The electric current density incident on the Moon has contributions from the plasma electrons (J_e) and ions (J_i), and the photoemission of electrons (J_{ph}) by solar UV and X-rays. The lunar surface will reach a potential such that the net incident current is zero, i.e., $J_e + J_i + J_{ph} = 0$. The current density equations are different for positive ($\phi_s > 0$) and negative ($\phi_s < 0$) surface potentials (see Appendix of Manka, 1973). To determine J_{ph} we assume the photocurrent density from normally incident sunlight to be $j_{ph} = 4.0 \times 10^{-5} \text{ A m}^{-2}$ (Goertz, 1989; Manka, 1973). J_{ph} is then calculated for a lunar surface photoelectron efficiency of $\eta = 0.1$, which is typical for dielectrics (Goertz, 1989). J_{ph} varies with the angle from the subsolar point, θ , and so is highest at the equator at local noon ($\theta = 0^\circ$) and drops off to zero at the terminator ($\theta = 90^\circ$).

Assuming one-dimensional Debye shielding above a plane, the lunar surface electric field is

$$E_s = \frac{\phi_s}{\lambda_D}. \quad (1)$$

Once the dust grain leaves the surface, the net upward force acting on it is $F = F_q - F_g$. The charge on a dust grain, q , is simply given by $q = C\phi_s$, where C is the grain capacitance. If we assume that the dust grains are spheres of radius r_d , and that $r_d \ll \lambda_D$, then the grain capacitance is given by $C \approx 4\pi\epsilon_0 r_d$ (Goertz, 1989).

The net acceleration acting on a dust grain in the sheath region is $a_{sh} = a_q - g_L$, where a_q is the electrostatic acceleration and g_L is the acceleration due to lunar gravity (assumed to be constant near the surface). Levitating models assume a priori that $a_{sh} \approx 0$, but here we relax that constraint to include dynamic motion. Assuming a_q is uniform and acts only in a sheath region of height λ_D above the surface, then it can be expressed as

$$a_q = \frac{qE_s}{m} = \frac{3\epsilon_0\phi_s^2}{\rho\lambda_D r_d^2}, \quad (2)$$

where m is the dust grain mass, and ρ is the dust grain density (i.e., specific gravity of lunar dust $\times 10^3 \text{ kg m}^{-3}$).

The exit velocity (V_{exit}) from the top of the sheath is then given by

$$V_{exit}^2 = 2a_{sh}\lambda_D = 2g_L(Z_{MAX} - \lambda_D). \quad (3)$$

After leaving the sheath region, a dust grain follows a ballistic trajectory to a maximum height above the lunar surface of

$$Z_{MAX} = \frac{3\varepsilon_0\phi^2}{\rho g_L r_d^2}. \quad (4)$$

Note that this equation is only valid when $a_q > g_L$.

The time taken to reach Z_{MAX} can be expressed as

$$t_{MAX} = t_{sh} + t_{bal} = \frac{V_{exit}}{a_{sh}} + \frac{V_{exit}}{g_L} = \sqrt{\frac{2\lambda_D}{a_{sh}}} + \sqrt{\frac{2(Z_{MAX} - \lambda_D)}{g_L}}, \quad (5)$$

where t_{sh} is the time taken to travel through the sheath, and t_{bal} is the time taken to travel the remaining distance to Z_{MAX} in a ballistic trajectory.

If grain cohesion at the surface is neglected (see discussion in section 4), then the criteria for grain lofting ($a_q > g_L$), can also be given in terms of a maximum grain radius that can be lofted, r_{MAX} , such that the lofting condition can be expressed as

$$r_d < r_{MAX} = \sqrt{\frac{3\varepsilon_0}{\rho g_L \lambda_D}} |\phi_S|. \quad (6)$$

Dust grains with radii that exceed r_{MAX} will either be levitated by the static mechanism discussed previously or will remain on the surface.

3. Model results

Here we have used the equations for lunar dust charging and dynamics, described in section 2, together with electron data from Lunar Prospector (courtesy of J.S. Halekas), to calculate Z_{MAX} (Fig. 4a) and the time taken to reach Z_{MAX} (Fig. 4b) as a function of r_d . In Fig. 5 we also show Z_{MAX} as a function of r_d and θ . The values for various parameters used in the calculations are

shown in Tables 1 and 2. We use the average electron concentrations (n_e) and temperatures (T_e) measured by the Electron Reflectometer aboard Lunar Prospector (LP) while the Moon was in the solar wind (Halekas et al., 2002). As LP was in such close proximity to the lunar surface (20–40 km altitude), it was used in preference to one of the usual upstream monitors, such as ACE or Wind. In fact, Table 2 shows that the n_e and T_e observed by LP varied as a function of θ . Using this data we estimate ϕ_S , λ_D , E_S and r_{MAX} at the subsolar point ($\theta \approx 0^\circ$), in an intermediate region ($\theta \approx 45^\circ$) and at the terminator ($\theta \approx 90^\circ$), as shown in Table 2. As there is no ion data from LP we assume that (1) the plasma near the Moon is quasi-neutral and (2) the electrons and ions have the same temperature, i.e., $n_i = n_e$ and $T_i = T_e$.

Like Manka (1973), we also found that the surface charging on the dayside is driven by the photoelectron currents (photo-driven) and so charges positive; while on the nightside it is the plasma electron currents that dominate (electron driven) and the surface there charges negative. Due to the lower plasma concentrations, the nightside currents are much weaker. From Table 2, one can see that the surface potentials on the dayside are $\approx +4$ V and on the nightside are ≈ -40 V, differing in magnitude by about a factor of 10. The Debye lengths used in this model are for the species attracted to the lunar surface, i.e., on the dayside, where $\phi_S > 0$, we use the electron Debye length (λ_{De}), and vice versa. It is important to note that the dominant source of electrons on the lunar dayside is from photoemission (at $\sim 500 \text{ cm}^{-3}$ this is ~ 100 times greater than electron concentrations in the solar wind). Therefore, photoelectrons are used to calculate the local Debye length. From Table 2 we can see that E_S at the subsolar point is greater than E_S at the terminator; this is due in part to the shorter λ_D .

The radius of the maximum size grain to be lofted, r_{MAX} , peaks at the terminator at almost 1 μm . This peak in grain size at the terminator is due to a combination of large ϕ_S (also causing the dust grains to carry a higher charge, since $q \propto \phi_S$) and relatively large E_S , which together produce a maximum in F_q acting on the dust grains.

Fig. 4 shows Z_{MAX} and the time taken to reach Z_{MAX} as a function of r_d at the subsolar point (dark grey dashed-lines), in the intermediate region (light grey lines), and at the terminator (black lines). From Fig. 4a one can see that the maximum heights reached for the smaller dust grains are ≈ 1.0 km at the subsolar point and ≈ 100 km at the terminator, while Fig. 4b shows that they are

lofted to Z_{MAX} on timescales of ≈ 30 to ≈ 300 seconds, respectively. This figure shows that the dynamic dust fountain model can account for submicron dust at altitudes up to ~ 100 km, and that the times taken to reach Z_{MAX} are consistent with the astronaut observations of the horizon glow and streamers varying on timescales of seconds to minutes, as sketched in Fig. 1. We also notice that Z_{MAX} is lowest in the intermediate region, thus indicating that a minimum exists between $\theta \approx 45^\circ$ and $\theta \approx 90^\circ$, which we shall discuss later.

In Fig. 4b one can see that the dust grain travel times to Z_{MAX} tend toward infinity as grain sizes approach the r_{MAX} lofting limit. This shows that static dust grain levitation is the limiting case of our dynamic model. Note that the model predictions are not as accurate for the static levitation case as for the dynamic case, since we have assumed that E_S is uniform and acts only within a Debye length from the surface, as discussed in section 2 and indicated in Figs. 2 and 5. However, this could be easily rectified in a more sophisticated model based on the same physical principles. We focus here on the dynamic case.

Fig. 5 shows Z_{MAX} as a function of r_d and θ , which reveals that dust may be lofted by the fountain effect at most locations on the lunar surface. However, there is an absence of lofted dust in a region just sunward of the terminator ($\theta \approx 80^\circ$), which we refer to here as the “Dead Zone”. In our model this is the location of the transition from $\phi_S > 0$ on the dayside to $\phi_S < 0$ on the nightside, so there is no net charging of the surface ($\phi_S \approx 0$). Hence, no lofting of dust grains can occur there.

4. Discussion

From the results presented in section 3 it appears that the dynamic fountain model described in section 2 is a viable mechanism for lofting dust grains from the lunar surface to altitudes from < 1.0 m to 100 km, as shown in Figs 4 and 5. In fact, at the terminator we predict that $\sim 0.01 \mu\text{m}$ dust grains are able to reach ~ 100 km, under average solar wind conditions, which is consistent with the observations discussed in section 1. However, it is important to note that we have made some simplifying assumptions (detailed in section 2) and neglected some effects that could possibly be more significant.

The cohesion of dust at the surface has been neglected here since, according to Rhee et al. (1977), when the electrostatic stress on a grain ($F_s = \epsilon_0 \phi_s^2 r_d^{-2}$) exceeds the soil cohesion (F_{coh}) it no longer coheres to the surface. Lunar soil cohesion varies between 0.1 and 1.0 kPa (Mitchell et al., 1972; Heiken et al., 1991 and references therein), and so for the grain sizes and surface potentials relevant here it can be argued that submicron dust grains do not stick to the surface since $F_s \gg F_{coh}$ is always the case. However, more recent work by Starukhina (2000) suggests that it may be necessary to consider the importance of contact forces between individual dust grains, arising from capillary forces, in order to better model the cohesion of dust grains at the surface.

Solar wind electrons striking the lunar surface are energetic enough to ionize it, thus producing secondary electrons which represent a positive charging current (Goertz, 1989; Horányi, 1996). Secondary electron currents, although neglected here, were considered by Manka (1973), but there was significant uncertainty in their overall contribution. More recently, however, Horányi et al. (1998) have conducted laboratory experiments on Apollo 17 lunar dust samples and have better determined the energy-dependence of the secondary electron currents produced. Including secondary currents in a surface charging model would add significant complication, but the experimental results are available to make reasonable estimates.

In our model we have only considered the vertical component of E_S and neglected any horizontal component. Horizontal electric fields will be created between regions of different potential, and we would expect such fields to be most noticeable near the transition from $\phi_s > 0$ to $\phi_s < 0$. Berg (1978) suggested that horizontal electric fields would be created at the terminator, between sunlit and dark regions of the surface, in order to explain the LEAM results discussed in section 1.

On a global scale the Moon is effectively an unmagnetised dielectric body, therefore its interaction with the solar wind forms a void or “lunar wake” in the anti-sunward direction (Ogilvie et al., 1996). The plasma density in the wake decreases exponentially from the edge toward the center. Ogilvie et al. (1996) observed two distinct cold ion beams refilling the lunar wake. Simulations by Farrell et al. (1998) have shown that the ion beams were generated by ambipolar electric fields formed at the wake edges, i.e. at the terminator. Therefore it appears

that a thorough understanding of lunar surface charging at the terminator and on the nightside requires the consideration of effects due the formation and refilling of the lunar wake.

As the density of dust grains lofted above the lunar surface appears to be quite low, we have assumed that the grains are shielded from one another, and as such do not act collectively. Using the McCoy (1976) model “0”, Murphy and Vondrak (1993) estimated the vertical dust column concentration, integrated over all grain radii, to be $\sim 2 \times 10^5 \text{ cm}^{-2}$. When dust in a plasma acts collectively it is referred to as a “dusty plasma” and this has significant effects on the properties of the dust grains and the plasma (Sukla and Mamun, 2002). Specifically, when dust concentrations are high, there is a tendency to have a reduction in individual grain charging due to collective effects (Goertz, 1989; Sukla and Mamun, 2002). Such a reduction in grain charge was not considered here.

In the lunar dust fountain model we have identified the dominant factors in the lofting of submicron grains to altitudes from tens of centimeters to hundreds of kilometers above the lunar surface. This process is driven by the charging of the lunar surface and dust grains by the solar wind plasma and the photoemission of electrons, which causes the like-charged surface and dust to repel each other, such that the dust is lofted to great heights. Simplifying assumptions have been that ϕ_s is shielded within one Debye length from the surface, and that the grain leaves the surface carrying the maximum amount of charge for the given ϕ_s . This has allowed us to include the most important physics as well as to have an intuitive understanding of the results. Our model demonstrates the feasibility of dynamic grain behaviour; however, future models will include the effects discussed above (if they prove to be significant) in order to improve our understanding of this phenomenon and further refine predictions of Z_{MAX} .

5. Summary and Conclusions

In analysis of lunar horizon glow and streamers caused by charged dust grains, the static levitation theories account for $\approx 5 \mu\text{m}$ grains at $\sim 10 \text{ cm}$ above the surface, but they cannot explain the $\sim 0.1 \mu\text{m}$ grains at altitudes of $\sim 100 \text{ km}$. The simple dynamic dust grain fountain model presented here is a viable mechanism for lofting $\sim 0.01\text{--}0.1 \mu\text{m}$ grains to altitudes $\sim 0.1\text{--}100 \text{ km}$ at the terminator. This is consistent with observations of this phenomenon described in section 1. As expected, the smallest grains reach the highest altitudes, as shown in Fig. 5.

Surface charging is driven by photoelectron currents on the dayside and plasma electron currents on the nightside, which affects the grain lofting heights. A region where no lofting of dust grains occurs, referred to here as the “Dead Zone”, is formed at the transition from $\phi_s > 0$ to $\phi_s < 0$, as shown Fig. 5. The surface potential in the Dead Zone region falls to ≈ 0 V, so there is neither enough charging, nor a strong enough electric field to lift grains from the surface. The location of the Dead Zone will obviously vary depending on conditions, but we predict that when the Moon is in the solar wind it will typically occur just dayside of the terminator ($\theta \approx 80^\circ$).

In the model presented here we have neglected the effects of: (1) grain cohesion at the surface, (2) secondary electron currents, (3) horizontal electric fields at the terminator, (4) the lunar wake on surface charging near the terminator, (5) collective behaviour on dust grain charging. Of these, we would expect grain cohesion at the surface to have the most significant impact. Further improvements would also include a more realistic treatment of the surface electric field, which should decay exponentially above the surface due to Debye shielding.

Our model predicts that a lunar orbiting spacecraft with a charged dust detector, such as SMART-1 (Tajmar *et al.*, 2002), would observe very small ($\ll 0.01 \mu\text{m}$) positively charged grains above the dayside, a region in the Dead Zone where no detection occurs, and larger (0.01–0.1 μm) negatively charged grains around the terminator region.

From a comparison of our results with the work of Murphy and Vondrak (1993) it appears that submicron dust grains could contaminate astronomical observations of infra-red, visible and UV light over the majority of the lunar surface, and not just at the terminator. This is one of many ways in which dust could interfere with science and exploration activities on the Moon; therefore a thorough understanding of lunar dust behaviour is necessary in order to effectively tackle these problems in the future.

Acknowledgements

T.J. Stubbs was funded by a National Research Council award at NASA/GSFC. We would like to thank J.S. Halekas for providing us with electron data from Lunar Prospector, and for useful discussions about lunar surface charging. Figures 1 and 3 reproduced courtesy of J.E. McCoy.

Stubbs, T.J., *et al.*, A dynamic fountain model for lunar dust, *Adv. Space Res.*, in press, 2005.

References

Berg, O.E., Wolf, H., Rhee, J.W. Lunar soil movement registered by the Apollo 17 cosmic dust experiment, in: Elsässer, H., Fechtig, H. (Eds.), *Interplanetary Dust and Zodiacal Light*.

Springer-Verlag, Berlin, pp. 233-237, 1976.

Berg, O.E., A lunar terminator configuration, *Earth Planet. Sci. Lett.*, 39, 377-381, 1978.

Criswell, D.R. Horizon-glow and the motion of lunar dust, in: Grard, R.J.L. (Ed.), *Photon and Particle Interactions with Surfaces in Space*. D. Reidel Publishing Co., Dordrecht, Holland, pp. 545-556, 1973.

Farrell, W.M., Kaiser, M.L., Steinberg, J.T., *et al.* A simple simulation of a plasma void: Applications to Wind observations of the lunar wake, *J. Geophys. Res.*, 103, 23653-23660, 1998.

Goertz, C.K. Dusty plasmas in the solar system, *Rev. Geophys.*, 27, 271-292, 1989.

Heiken, G.H., Vaniman, D.T., French, B.M. *Lunar Sourcebook a User's Guide to the Moon*, Cambridge University Press, 1991.

Halekas, J.S., Mitchell, D.L., Lin, R.P., *et al.* Evidence for negative charging of the lunar surface in shadow, *Geophys. Res. Lett.*, 29(10), 1435, doi:10.1029/2001GL014428, 2002.

Horányi, M. Charged dust dynamics in the solar system, *Annu. Rev. Astron. Astrophys.*, 34, 383-418, 1996.

Horányi, M., Walch, B., Robertson, S., *et al.* Electrostatic charging properties of Apollo 17 lunar dust, *J. Geophys. Res.*, 103, 8575-8580, 1998.

Manka, R.H. Plasma and potential at the lunar surface, in: Grard, R.J.L. (Ed.), *Photon and Particle Interactions with Surfaces in Space*. D. Reidel Publishing Co., Dordrecht, Holland, pp. 347-361, 1973.

McCoy, J.E., Criswell, D.R. Evidence for a high altitude distribution of lunar dust, *Proc. Lunar Sci. Conf. 5th*, 2991-3005, 1974.

Stubbs, T.J., *et al.*, A dynamic fountain model for lunar dust, *Adv. Space Res.*, in press, 2005.

McCoy, J.E. Photometric studies of light scattering above the lunar terminator from Apollo solar corona photography, *Proc. Lunar Sci. Conf.* 7th, 1087-1112, 1976.

Mitchell, J.K., Houston, W.N., Scott, R.F., *et al.* Mechanical properties of lunar soil: Density, porosity, cohesion and angle of friction, *Proc. Lunar Sci. Conf.* 3rd, 3235–3253, 1972.

Murphy, D.L., Vondrak, R.R. Effects of levitated dust on astronomical observations from the lunar surface, *Proc. Lunar Planet. Sci. Conf.* 24th, 1033–1034, 1993.

Ogilvie, K.W., Steinberg, J.T., Fitzenreiter, R.J., *et al.* Observations of the lunar plasma wake from the Wind spacecraft on December 27, 1994, *Geophys. Res. Lett.*, 23, 1255-1258, 1996.

Rennilson, J.J., Criswell, D.R. Surveyor observations of lunar horizon-glow, *The Moon*, 10, 121-142, 1974.

Rhee, J.W., Berg, O.E., Wolf, H. Electrostatic dust transport and Apollo 17 LEAM experiment, in: *COSPAR Space Research XVII*. Pergamon, New York, pp. 627-629, 1977.

Starukhina L. V. Characteristics of the contact between regolith particles: the influence on the physical properties of regoliths. *Solar System Research*, 34, 4, 295-302, 2000.

Sukla, P.K., Mamun, A.A. *Introduction to Dusty Plasma Physics*, Institute of Physics Publishing, Bristol, 2002.

Tajmar, M., Gonzalez, J., Saccoccia, G., *et al.* Plasma diagnostics and simulation for the SMART-1 mission, *Planet. Space Sci*, 50, 1355–1360, 2002.

Whipple, E.C. Potentials of surfaces in space, *Rep. Prog. Phys.*, 44, 1197–1250, 1981.

Zook, H.A., McCoy, J.E. Large scale lunar horizon glow and a high altitude lunar dust exosphere, *Geophys. Res. Lett.*, 18, 11, 2117-2120, 1991.

Tables

Table 1. Values used in the lunar dust charging and dynamics equations.

Parameter	Value used	Data source
Lunar gravity, g_L	1.62 m s^{-2}	Heiken et al., 1991
Dust grain mass density, ρ	$3.0 \times 10^3 \text{ kg m}^{-3}$	Heiken et al., 1991
Solar wind flow velocity, V_{sw}	400 km s^{-1}	Typical value used in the literature
Photoelectron current, j_{ph}	$4.0 \times 10^{-5} \text{ A m}^{-2}$	Goertz, 1989; Whipple, 1981
Photoemission efficiency, η	0.1	Goertz, 1989; Whipple, 1981
Photoelectron temperature, T_{ph}	$1.74 \times 10^4 \text{ K}$	Goertz, 1989; Whipple, 1981

Table 2. Lunar Prospector electron data and results from the dynamic fountain model as a function of angle from the subsolar point.

Parameters	Subsolar point	Intermediate region	Terminator
Angle from subsolar point, $\theta / ^\circ$	0 – 6	42 – 48	90 – 96
LP plasma electron density, n_e / cm^{-3}	2.9	4.0	7.0
LP plasma electron temperature, T_e / K	1.4×10^5	1.5×10^5	1.1×10^5
Surface potential, ϕ_S / V	+4.1	+3.1	-36
Surface Debye length, λ_D / m	0.41	0.72	8.6
Surface electric field, $E_S / \text{V m}^{-1}$	+9.9	+4.2	-4.1
Maximum dust grain radius lofted, $r_{MAX} / \mu\text{m}$	0.47	0.26	0.90

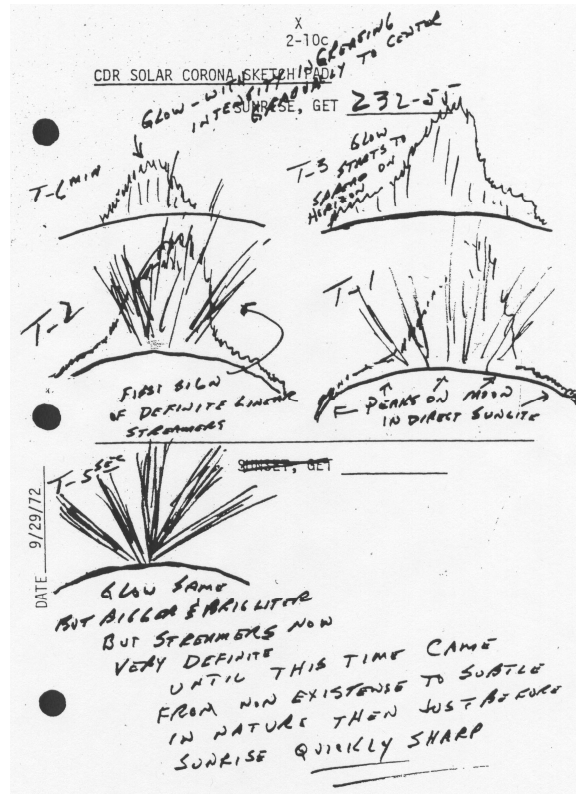


Fig. 1. Sketches of sunrise with “horizon glow” and “streamers” viewed from lunar orbit by astronaut E.A. Cernan (commander) during the Apollo 17 mission. The time in minutes (T-6 min, T-3, T-2, T-1) and seconds (T-5 sec) before the first appearance of the Sun is indicated (McCoy and Criswell, 1974).

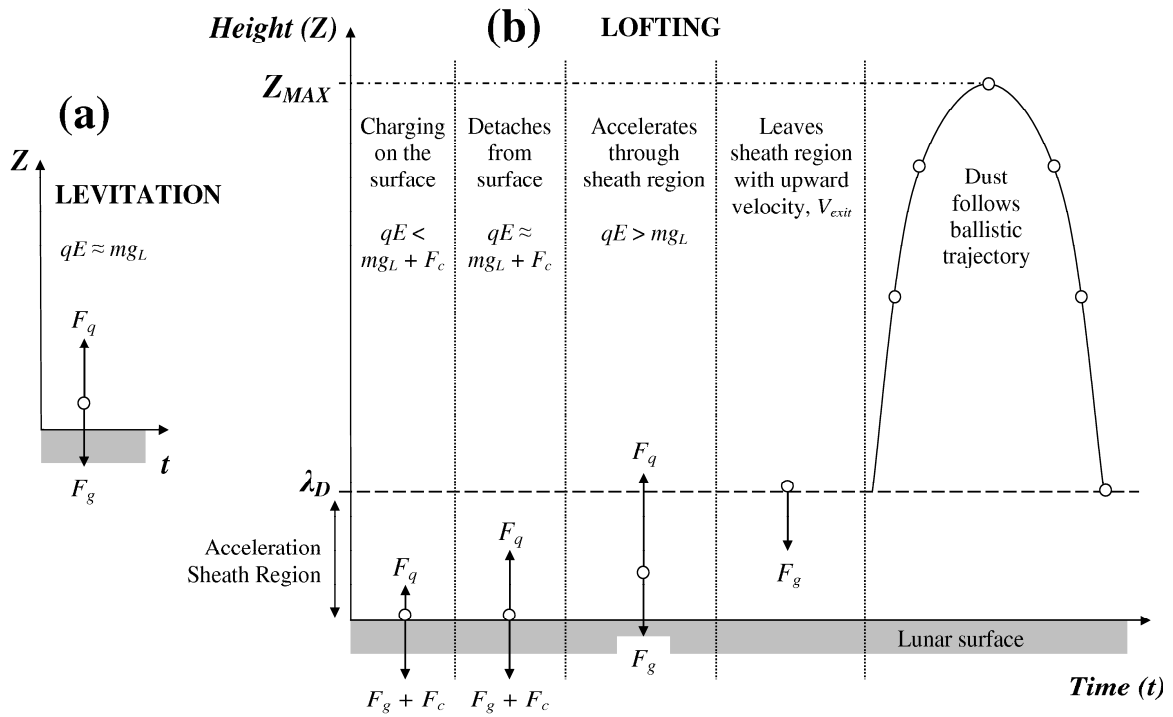


Fig.2. Schematic comparing (a) the static levitation concept, as suggested by Criswell (1973) and others, with (b) the evolution of a dust grain in our dynamic fountain model.

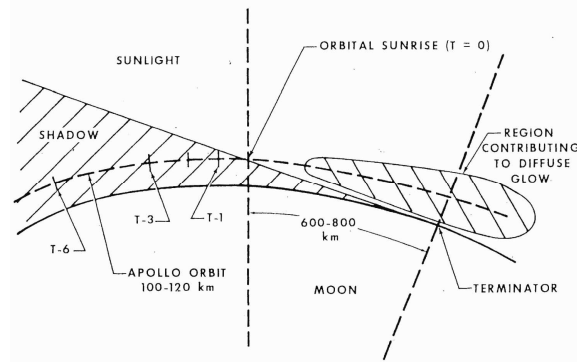


Fig. 3. Schematic from McCoy (1976) showing a cross-section of the Moon in the plane of the Apollo orbit (dashed line). This depicts the physical situation consistent with the observations shown in Fig. 1.

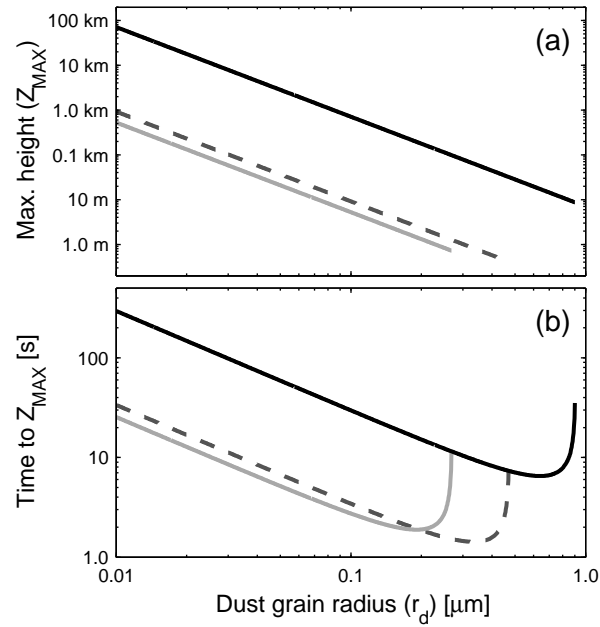


Fig. 4. Predictions of (a) the maximum height reached above the surface (Z_{MAX}) and (b) the time taken to reach Z_{MAX} as a function of dust grain radius (r_d), as predicted at the subsolar point (dark grey dashed-lines), in an intermediate region (light grey lines), and at the terminator (black lines).

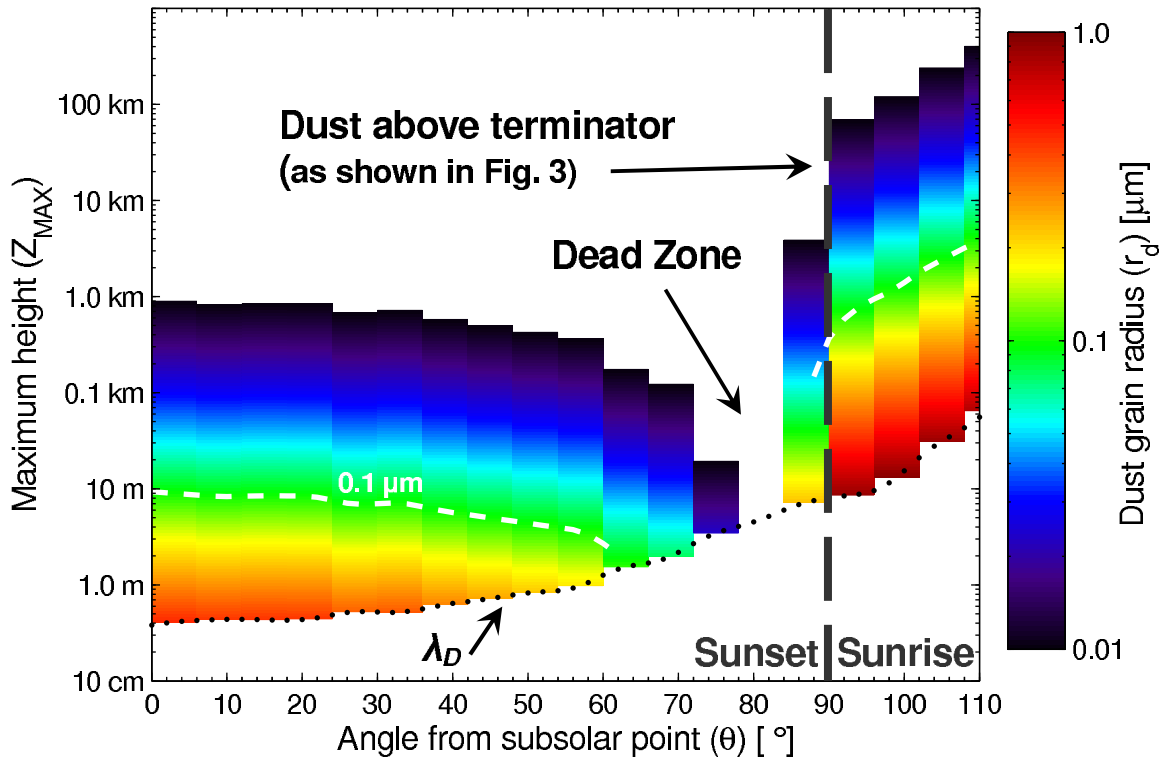


Fig. 5. Spectrogram plot showing fountain model predictions for the maximum dust grain height reached (Z_{MAX}) as a function of angle from the subsolar point (θ) and dust grain radius (r_d). The contour for the predicted altitude reached by 0.1 μm dust grains is indicated by the broken white line. The Debye length (λ_D) is represented by the black dotted line, and marks the extent of the “Acceleration Sheath Region” in this model (see Fig. 2).